EARTHQUAKE ENGINEERING AND STRUCTURAL DYNAMICS
Earthquake Engng Struct. Dyn. 2005; **34**:393–408
Published online 14 January 2005 in Wiley InterScience (www.interscience.wiley.com). DOI: 10.1002/eqe.446

Performance evaluation of shear links and orthotropic bridge deck panels for the new San Francisco–Oakland Bay Bridge

Chia-Ming Uang[1,*,†], Frieder Seible[1], Cole McDaniel[2] and Chung-Che Chou[3]

[1]*Department of Structural Engineering, University of California at San Diego, La Jolla, CA 92093, U.S.A.*
[2]*Department of Civil and Environmental Engineering, Washington State University, Pullman, WA 99163, U.S.A.*
[3]*Department of Civil Engineering, National Chiao Tung University, Hsinchu 300, Taiwan*

SUMMARY

This paper presents results from testing and the associated analytical studies of steel shear links and orthotropic bridge decks to support the design of the new East Span for the San Francisco–Oakland Bay Bridge. Cyclic testing of full-scale built-up links showed that the specimens were able to reach an inelastic rotation more than twice that which would be produced from a 1500-year Safety Evaluation Earthquake event. Nevertheless, brittle fracture occurred before the inelastic design rotation capacity, as specified in the AISC Seismic Provisions, was developed. Based on a parametric study, a modification to the welding details was proposed, which proved to be effective in preventing this type of fracture in a subsequent testing program. Monotonic testing of two reduced-scale orthotropic bridge deck panels, one stiffened with closed ribs and another one with open ribs, also showed that these specimens could develop a compression capacity greater than that which would be produced by the design earthquake. The post-buckling behavior was associated with the buckling direction and the type of ribs. Copyright © 2005 John Wiley & Sons, Ltd.

KEY WORDS: San Francisco–Oakland Bay Bridge; shear link; orthotropic deck; brittle fracture; buckling; welding

INTRODUCTION

The East Span of the new San Francisco–Oakland Bay Bridge (SFOBB), designed by the joint venture of T.Y. Lin International and Moffatt & Nichol [1], is a 565 m long, single tower, steel self-anchored suspension bridge with a main span of 385 m (Figure 1). The tower of the bridge consists of four steel shafts interconnected in the transverse and longitudinal

*Correspondence to: Chia-Ming Uang, Department of Structural Engineering, University of California at San Diego, La Jolla, CA 92093, U.S.A.
†E-mail: cmu@ucsd.edu

Contract/grant sponsor: California Department of Transportation (Caltrans)

Received 28 March 2004
Revised 12 September 2004
Accepted 5 October 2004

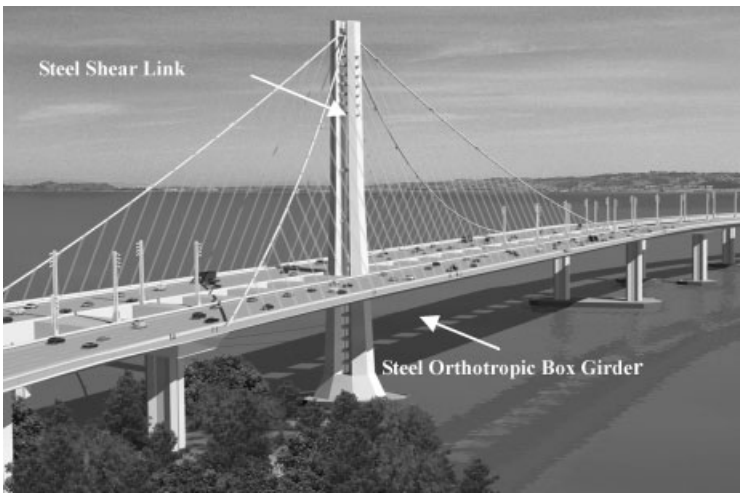

Figure 1. The new SFOBB East main span.

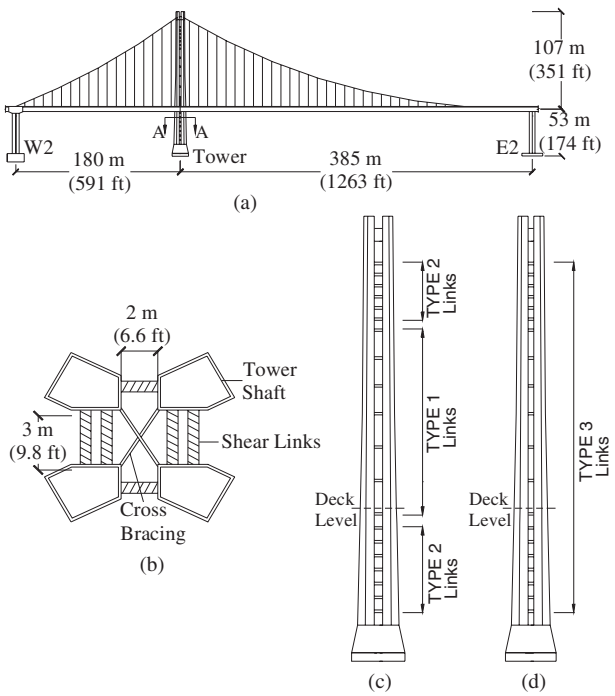

Figure 2. Tower cross-section and elevations: (a) main span elevation; (b) section A–A; (c) transverse tower elevation; and (d) longitudinal tower elevation.

directions by replaceable steel shear links (Figure 2). The suspension cable loops around the west bent and anchors to the bridge deck at the east bent; floor beams are spaced at 5 m inside the box girders. These box girders (Figure 3), a key component of the load-resisting

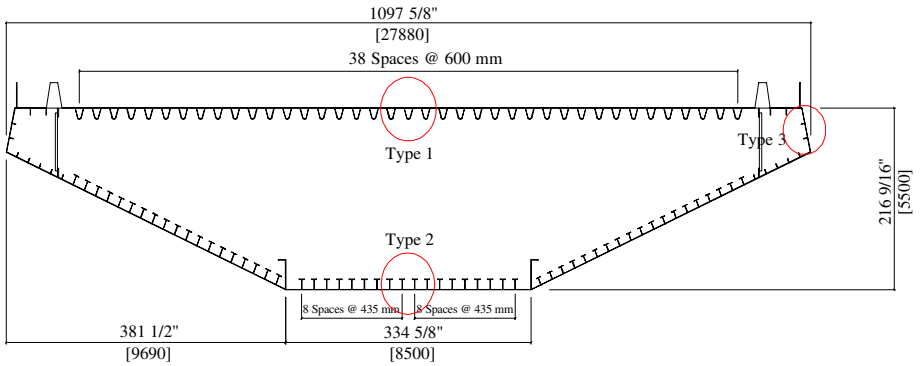

Figure 3. Main span girder cross-section.

system, balance the cable tension forces in compression. Three different types of longitudinal ribs (troughs, structural tees, and flat plates) are used to stiffen the girder plates such that the yield strength of the girder section can be developed. The tower shafts and box girders are designed to remain elastic under the Safety Evaluation Earthquake (SEE) with a return period of 1500 years, while the shear links are designed to deform inelastically to protect the tower shafts from damage.

Large-size testing of steel components was conducted at the University of California, San Diego to support the design of the SFOBB. The testing program was composed of two parts. First, full-scale tests of two built-up wide-flange shear links were conducted to evaluate the force and deformation characteristics under cyclic loading. Second, monotonic tests were conducted on two reduced-scale orthotropic decks that simulated a portion of the top and bottom decks of the main span box girders to assess the ultimate compressive strength and post-buckling behavior.

SHEAR LINK STUDY

The objectives of this test program were: (1) to evaluate the cyclic force and deformation characteristics of the full-scale built-up links, and (2) to evaluate the cyclic overstrength of the links, which is needed for capacity design of the towers and the link connections to towers.

Test specimens

Two full-scale shear link specimens were tested; one transverse link, Type 1, and one longitudinal link, Type 3 (see Figure 2). The shear links were built-up steel wide-flange sections with a shear 'deformable region' in the center and a 'connection region' on either side. Figure 4 shows the details of the Type 1 specimen. The connection region was defined as the portion outside the deformable region. The cross-section dimensions were the same for both link types except for a variation in flange width (the flange width for the Type 2 link was 475 mm). The plates for the shear link deformable regions were A709

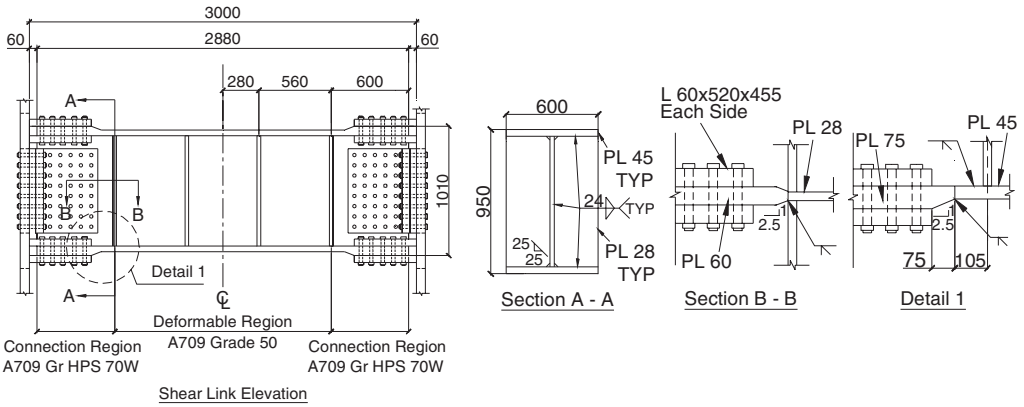

Figure 4. Link geometry and details (Type 1).

Table I. Link specimen material test results.

(a) Tensile coupon test results			
Plate	Yield strength (MPa)	Tensile strength (MPa)	Elong. based on 203 mm gauge length (%)
Web	354	497	25
Flange	366	532	27
(b) Charpy V-Notch test results			
Coupon	CVN (Joules)	Average (Joules)	
Flange at −22 °C	8		
	26	23	
	34		
Web at −12 °C	27		
	34	31	
	33		

Grade 50 steel with an additional requirement that the actual yield strength, as obtained from tensile coupon tests, did not exceed 379 MPa. This upper limit, included in the specifications for the new SFOBB, was introduced by the designers to ensure that the ultimate shear force in the links did not exceed the design capacity of the connection regions. Both tensile and Charpy V-Notch (CVN) tests for the steel plates in the deformable region were conducted. The measured material characteristics are summarized in Table I. The connection regions were made of A709 Grade HPS70W high-performance steel. A490 high-strength bolts, 30 mm in diameter, were used to splice the shear link flanges and webs to the columns.

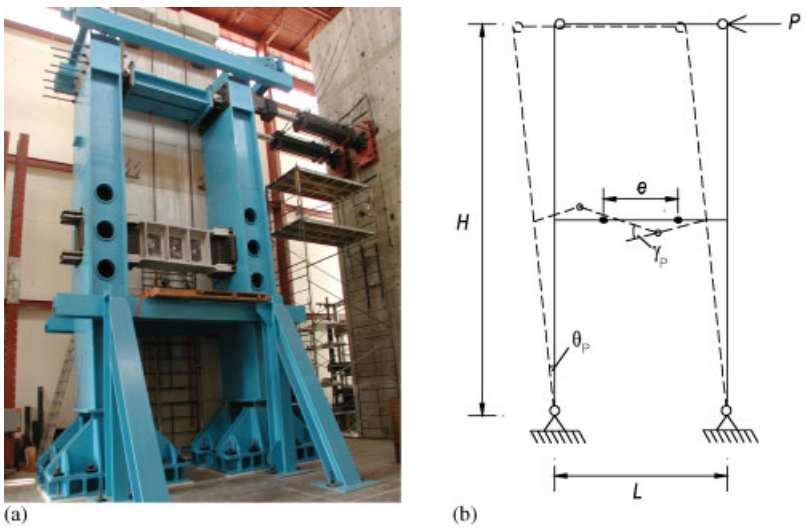

Figure 5. Shear link test set-up: (a) overall view; and (b) test setup geometry.

The links were designed in accordance with the AISC Seismic Provisions [2]. The length, e, of both links was less than $1.6M_p/V_p$, where V_p is the nominal shear strength and M_p is the nominal plastic flexural strength. Therefore, shear behavior is expected to dominate the response. To delay the onset of local buckling in the web, the designer provided intermediate stiffeners in the web such that the spacing was not more than $30t_w - d/5$, where t_w is the web thickness and d is the beam depth. According to the AISC Seismic Provisions, links thus designed would provide an inelastic design rotation capacity (γ_p) of 0.08 radian. Based on non-linear time-history analyses with the SEE event as the input ground motions, the designer predicted that the maximum inelastic rotation demands for the Type 1 and Type 3 links were only 0.01–0.02 radian and 0.03–0.04 radian, respectively.

The test specimens were fabricated by a commercial fabricator. The fabrication sequence was similar for both links. Once the plates were cut and prepped, the connection regions and deformable region of the flange plates were spliced together by complete joint penetration (CJP) groove welds. The same procedure was carried out for the web plate. Next, the flanges and web were welded together by CJP welds. Transverse stiffeners were then fillet welded to both sides of the web. All the shear link CJP groove welds were performed by the flux-cored arc welding process with E91T-1 electrodes for the Grade 70 material and E71T-1 for the Grade 50 material. The specified minimum CVN toughness for the welding electrodes was 34 J at $-30\,^{\circ}$C.

Test set-up

The test set-up was designed such that a large shear force demand can be applied to the full-scale specimens. Figure 5 shows that the set-up included two pin-based columns, a shear link specimen, an upper pinned strut, and a lateral restraint system.

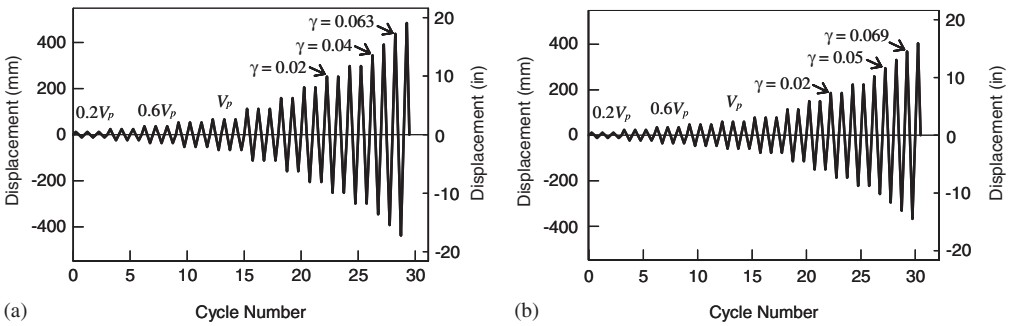

Figure 6. Link loading sequence: (a) type 1 shear link; and (b) type 3 shear link.

Loading sequence

The testing was conducted in a displacement controlled mode. A prescribed quasi-static cyclic loading sequence was imposed laterally to the top of the test set-up. The loading sequence was a variation of that proposed for testing link-to-column connections [2]. The loading protocol was followed until the inelastic rotation of the link exceeded that predicted from time history analyses by the designer. From then on, a single cycle at each deformation amplitude was imposed to the test specimen until the specimen failed. Such a modification was justified from results of time-history analysis, which indicated that the AISC loading protocol would unrealistically impose a very large cumulative inelastic deformation demand to the link specimens. (A recent study [3] also showed that the AISC loading protocol is very conservative.) Figure 6 shows the loading sequence that was imposed on the test specimens.

Test results

The behavior of the two specimens was similar. Minor flaking of the mill scale in the link web was visually identifiable in the early stage of testing. The first occurrence of slipping of the bolted flange splices, which was accompanied by a loud noise as the splice plates slid past the flanges, was observed during the first cycle when the imposed lateral displacement (Δ) was 66 mm. As the lateral displacement was increased, the splices continued to slip in both the push and pull directions. (Shear deformation of the deformable region was not affected by the bolt slippage because it occurred outside the region.) At 345 mm, cracks were visually observed at the ends of the vertical fillet welds connecting the intermediate stiffeners to the link web [see Figure 7(b)]. The cracks continued to propagate into the link web as the lateral displacement was increased. As the deformation was increased further, brittle fracture of the link web occurred [see Figure 8(a)]. A close-up at the crack initiation location is shown in Figure 9. A similar failure mode was also observed in the Type 3 link [see Figure 8(b)].

The link shear versus average shear deformation relationships of the deformable region are shown in Figure 10. Excluding the last incomplete cycle, the inelastic rotation reached 0.06 and 0.066 radians for the Type 1 and Type 3 links, respectively. The shear deformation in the connection regions was low, with the response remaining in the elastic range throughout the test.

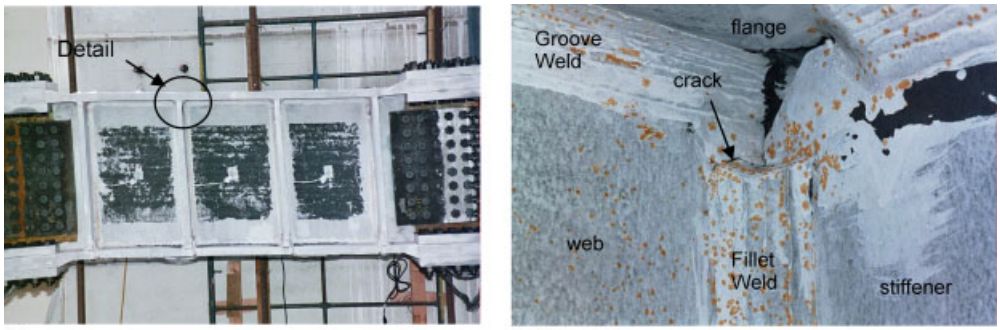

Figure 7. Type 1 link at $\Delta = 345$ mm: (a) deformed configuration; and (b) crack at end of stiffener/web fillet weld.

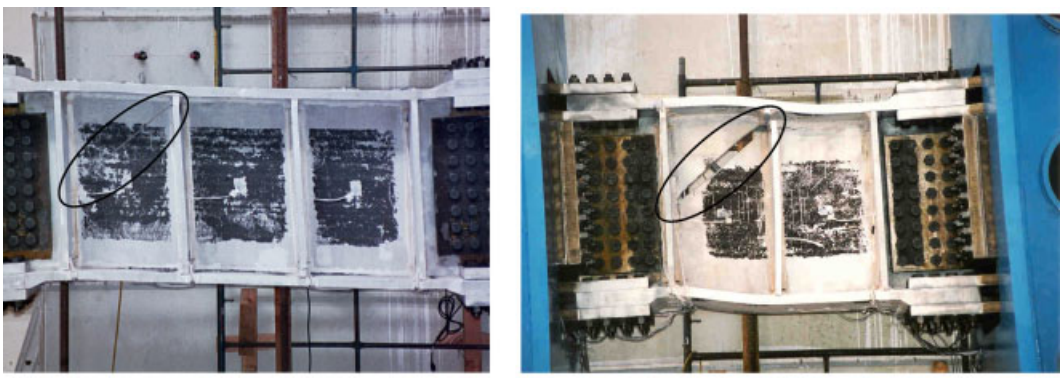

Figure 8. Brittle fracture of link specimens: (a) type 1 specimen; and (b) type 3 specimen.

The overstrength factor developed in each of the two test specimens was calculated by dividing the maximum shear strength by the plastic shear strength, which was based on the measured yield strength of the web material. The corresponding overstrength factors are 1.83 and 1.94, indicating that the value (1.25) recommended by the AISC Seismic Provisions for capacity design is non-conservative by a large margin. When thick flanges were used in the link, the contribution of flanges in resisting shear should be considered in evaluating the overstrength factor [4].

Crack prevention measures

The brittle fracture failure mode that occurred in such large-size built-up links had not been reported previously. The cracks in the two full-scale link specimens occurred at the ends of vertical welds of the intermediate stiffeners, near the highly restrained location where the flange-to-web groove weld, and the vertical and horizontal fillet welds of the stiffeners met (Figure 9). To mitigate the potential for crack initiation at the end of the fillet weld, one

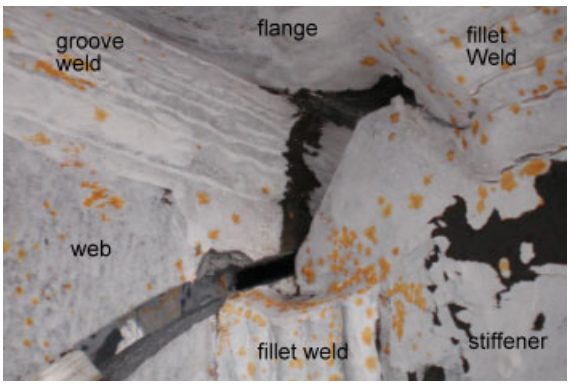

Figure 9. Close-up of crack initiation location (Link Type 1).

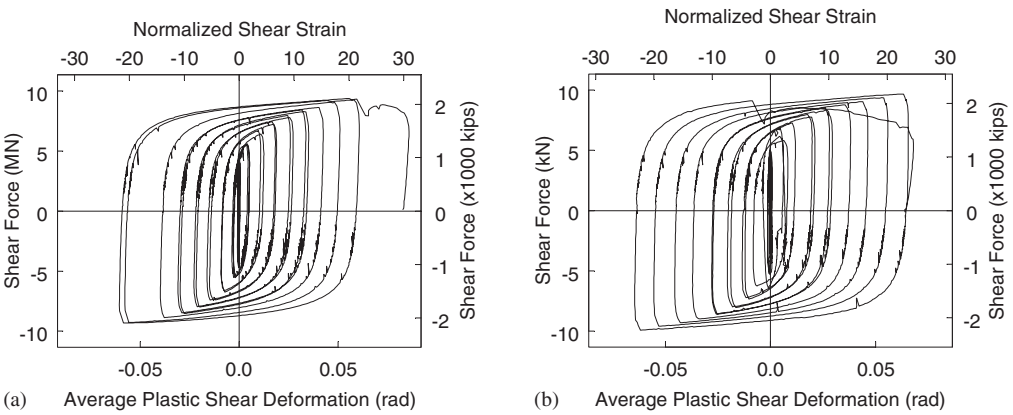

Figure 10. Link shear force versus inelastic rotation relationships: (a) type 1 specimen; and (b) type 3 specimen.

option is to terminate the welds further from the web-flange-stiffener intersection. The effectiveness of this scheme was explored by a series of 3D finite element analyses using the model similar to that shown in Figure 11(a); the non-linear finite element analysis computer program ABAQUS [5] was used for this purpose [6]. By varying the distance (c) from the end of the vertical fillet welds to the near toe of the web-to-flange [Figure 11(b)], the results showed that the hydrostatic stress and the effective plastic strain were reduced significantly when c was increased to about 5 times the web thickness (see Figure 12). It was also recommended that a smooth taper at the end of the fillet welds be provided. These recommendations, which were adopted for the fabrication of links for the SFOBB, were demonstrated later to be effective to avoid brittle fracture in another test program conducted at the University of Nevada, Reno [7].

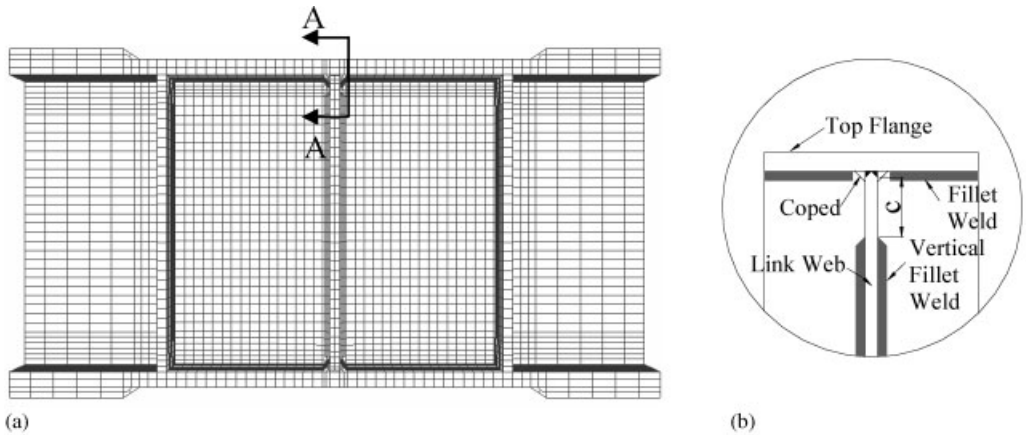

Figure 11. Finite element model: (a) elevation; and (b) detail A.

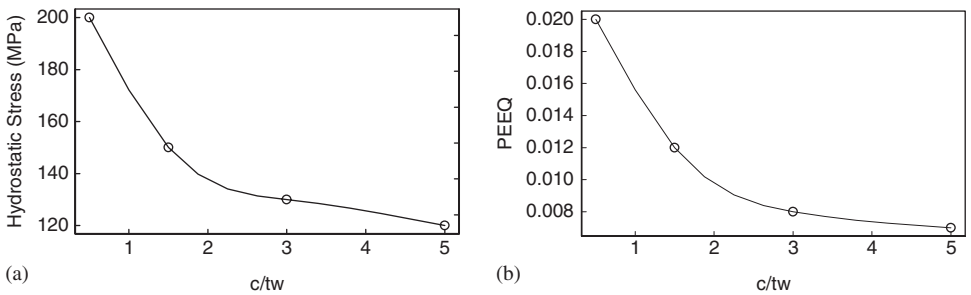

Figure 12. Link finite element analysis results: (a) hydrostatic stress; and (b) equivalent plastic strain.

ORTHOTROPIC BRIDGE DECK STUDY

The objective of this test program was to evaluate the ultimate compressive strength and post-buckling behavior of the longitudinally stiffened panels for the box girders. Unlike the cyclic testing of links that are expected to yield and dissipate energy during a major seismic event, monotonic testing was conducted on two reduced-scale stiffened panel models because the box girders are expected to remain elastic during an SEE event.

Test specimens

Portions of the top and bottom decks of a box girder (Figure 3) were investigated in this study. Since floor beams are spaced at 5 m on center inside the box girder, each deck can buckle longitudinally in an 'S' shape. To study the buckling behavior of the stiffened panels in both positive and negative bending directions, it was decided that each specimen include two spans. Reduced-scale models were tested due to the high force demand for testing. Figure 13

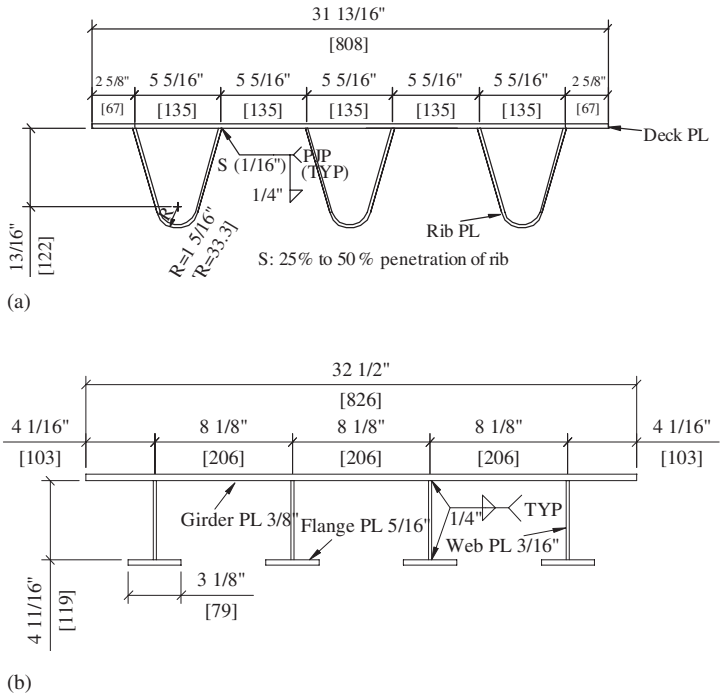

Figure 13. Cross-section of orthotropic bridge deck specimens: (a) specimen 1; and (b) specimen 2.

Table II. L deck specimen material properties.

Specimen no.	Plate	Thickness mm	Yield strength (MPa)	Tensile strength (MPa)	Elong. based on 203 mm gauge length (%)
1	Girder plate	6	372	510	20
	Rib plate	5	427	579	20
2	Girder plate	10	427	534	24
	Rib Web plate	5	427	579	20
	Flange plate	8	476	573	21

shows the cross-sections of both specimens. Specimen 1, with a scale factor of 0.45, was composed of three closed ribs and a top deck plate; Specimen 2, with a scale factor of 0.48, was made up of a bottom deck plate and four 'T'-shaped ribs.

The specimens were specified to be non-fracture critical members with ASTM A709 Grade 345 steel. Tensile material properties as obtained from the certified mill test reports are summarized in Table II.

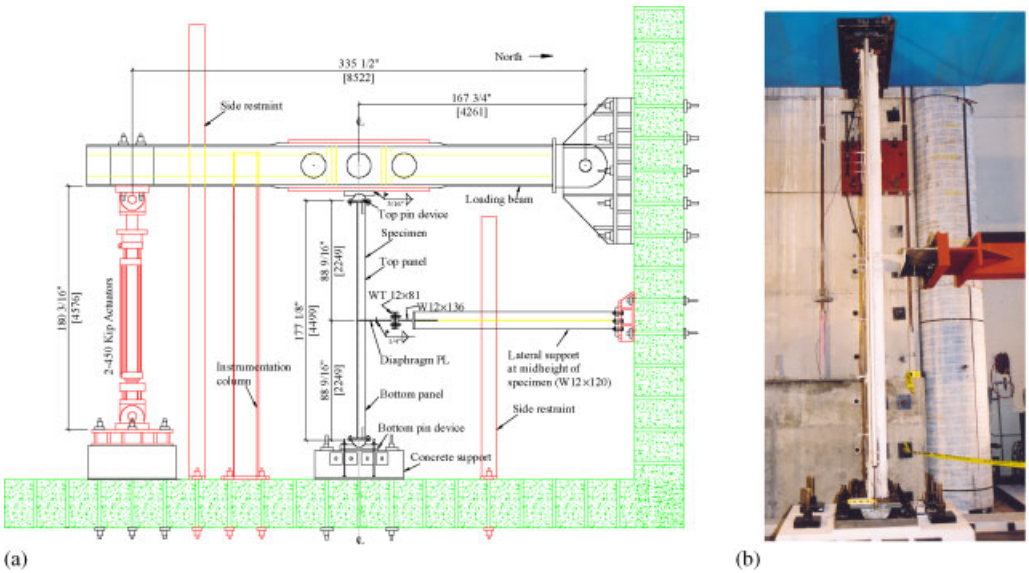

Figure 14. Bridge deck test set-up: (a) schematic; and (b) elevation.

Test set-up

The test set-up, shown in Figure 14, was composed of a horizontal loading beam, pin devices at both top and bottom ends, a specimen, and a concrete support. A lateral support connected by a diaphragm plate at the mid-height of the specimen was designed to simulate the lateral restraint provided by the floor beam.

A quasi-static, monotonic loading was applied to the specimen by using two 2000 kN actuators at one end of the loading beam. The testing was conducted in a displacement-controlled mode with axial deformation, Δ, of the specimen as the controlling variable.

Test results

The applied load versus axial deformation relationship of Specimen 1 is shown in Figure 15(a), in which both the yield capacity based on the actual yield strength and the seismic demand produced by an SEE event are marked. As the load was gradually applied, the maximum strength of the specimen was reached at $\Delta = 14\,\text{mm}$. The upper panel buckled in one direction and the lower panel buckled in the other direction, as shown in Figure 16(a). As the imposed axial deformation was increased further, local buckling of the deck plate across the width of the upper panel was observed, which then triggered rib buckling; the symmetric bulging buckling configuration of the ribs shown in Figure 16(b) was compatible in deformation with the buckling pattern of the deck plate. Figure 16(c) shows the buckling of the ribs that occurred near the upper end of the lower panel; note that the deck plate did not buckle. This buckling configuration is different from that shown in Figure 16(b) for the upper panel. The difference was primarily caused by the direction of bending after the maximum strength of the specimen was reached.

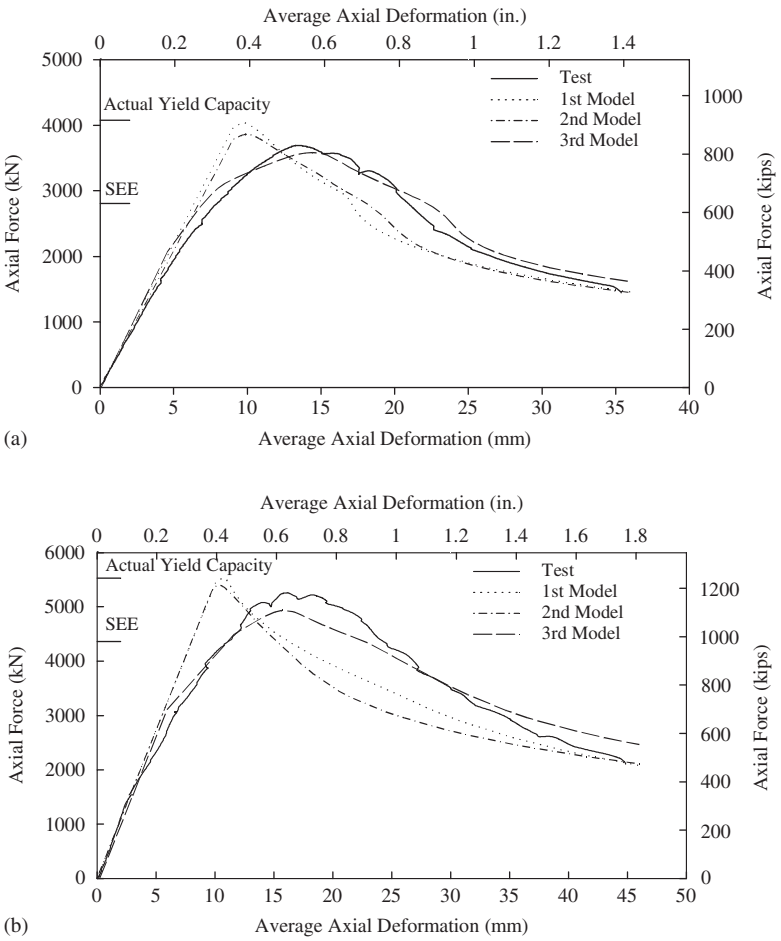

Figure 15. Applied load versus axial deformation relationships (bridge deck specimens): (a) specimen 1; and (b) specimen 2.

The applied load versus axial deformation relationship of Specimen 2 is shown in Figure 15(b), in which the SEE demand and actual yield capacity are also marked. The peak compression force was reached at $\Delta = 17$ mm, with the specimen buckled in reverse curvature as shown in Figure 17(a). Torsional buckling of the T-shaped ribs was observed in the lower panel of the specimen [see Figure 17(c)], but torsional buckling of the ribs was not observed in the upper panel [see Figure 17(b)]. Twisting of the specimen at the lower panel was also observed at the later stage of testing. It was due to the loss of torsional rigidity of the section after the T-shaped ribs experienced torsional buckling. No torsional buckling of the T-shaped ribs and twisting of the section was observed in the upper panel, but local buckling of the deck plate was observed between the intersection points of the web and girder plates.

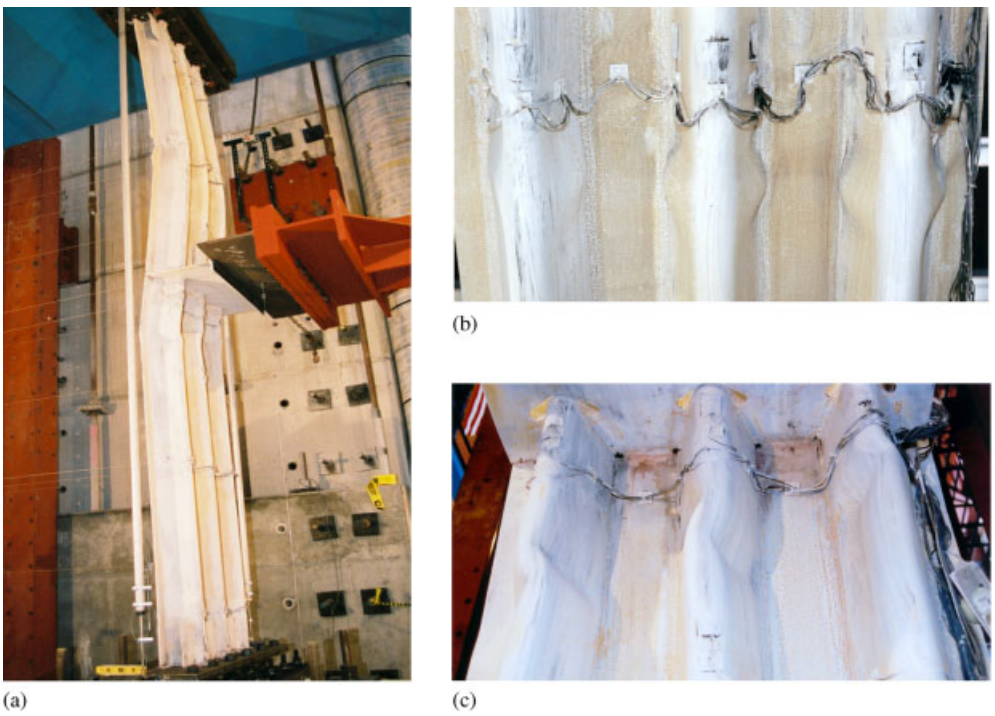

Figure 16. Deformed configurations after testing (Deck Specimen 1): (a) overall view; (b) upper panel; and (c) lower panel.

Figure 17. Deformed configurations after testing (Deck Specimen 2): (a) overall view; (b) upper panel; and (c) lower panel.

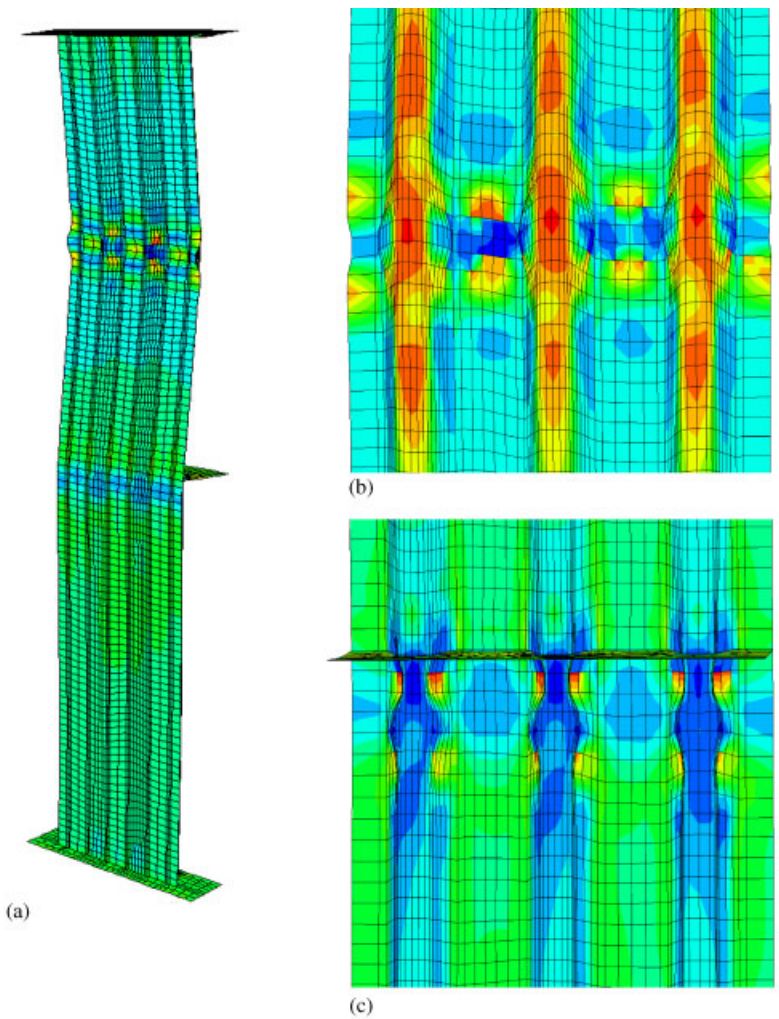

Figure 18. Predicted deformed configurations (Deck Specimen 1): (a) overall view; (b) upper panel; and (c) lower panel.

Finite element analysis

Specimens 1 and 2 were modeled using the non-linear finite element computer program ABAQUS [4] with the four-node doubly curved thin shell element S4R. Because the initial geometric imperfections and residual stresses have pronounced influences on the ultimate strength and post-buckling behavior of the stiffened panel, these two effects were considered in the study [8]. The measured geometric imperfection of each specimen was introduced by applying a uniform pressure perpendicular to the deck plate to mimic the deformed pattern and magnitude between the middle and end of the specimen. Three models were considered for each test specimen. Without considering the effects of both geometric imperfections and residual stresses, the first model shows that the actual yield capacity of the specimen could

be reached (see Figure 15) before strength degradation due to buckling. By considering only the initial geometric imperfections in the second model, the ultimate strength and elastic stiffness were slightly lower than that of the first model, but were higher than the test results. When both effects were considered, the third model predicted the ultimate strength and the post-buckling behavior reasonably well. The analysis also showed that the buckling modes could be simulated when the effects of geometric imperfections and residual stresses were considered (see Figure 18).

CONCLUSIONS

Large-size testing of steel components was conducted at the University of California, San Diego to support the design of the new East Span of the San Francisco–Oakland Bay Bridge. The testing program was composed of two parts. First, full-scale tests of two built-up wide-flange shear links were conducted to evaluate the force and deformation characteristics as well as the cyclic overstrength factor. Cyclic testing showed that both link specimens were able to reach an inelastic rotation greater than twice that which would be produced by a Safety Evaluation Earthquake event. Nevertheless, the inelastic rotation capacity did not reach that specified in the AISC Seismic Provisions due to brittle fracture of the link web, which initiated from a highly restrained region where several welds met. A parametric study using a non-linear finite element analysis program suggested that offsetting the stiffener-to-web fillet welds from the flanges by at least 5 times the web thickness would reduce the deformation demand in these susceptible areas. Providing a smooth taper at the end of the fillet welds was also provided. These recommendations proved to be beneficial in preventing brittle fracture in another testing program conducted later at the University of Nevada, Reno. The test results also showed that, for capacity design, the overstrength factor (1.25) as specified in the AISC Seismic Provisions is significantly lower than that measured (1.83 to1.94) and is, thus, non-conservative for the links tested.

The ultimate axial capacities of two reduced-scale, orthotropic bridge deck specimens were evaluated from monotonic loading. The full width of the girder plate in both specimens, stiffened longitudinally by the rib plates, reached yield before local buckling of the plate occurred. Both specimens reached a compression capacity greater than that which would be produced by a Safety Evaluation Earthquake event. After the ultimate strength was reached, the strength degradation of the first specimen, which was stiffened with closed ribs, was due to global buckling, local buckling of the lower-panel ribs and the upper-panel girder plate. For the second specimen, which was stiffened with open ribs, the strength degradation was initiated by torsional buckling of the lower-panel ribs, followed by the twisting of the lower panel and local buckling of the upper-panel girder plate. It was also found from numerical simulation that the residual stresses have more influence on the ultimate strength and post-buckling behavior than the geometric imperfections.

ACKNOWLEDGEMENTS

This research project was sponsored by the California Department of Transportation (Caltrans). Dr Wenyi Long served as the Project Contact. Dr Marwan Nader and Mr Laurent Rus of T.Y. Lin International provided information and guidance for the design and fabrication of the specimens.

REFERENCES

1. Tang M, Manzanarez R, Nader M, Abbas S, Baker G, Replacing the East Bay Bridge. *Civil Engineering* (ASCE) 2000; **70**(10):38–43.
2. AISC, *Seismic Provisions for Structural Steel Buildings*, American Institute of Steel Construction, Chicago, IL, 1997.
3. Richards P, Uang CM, Okazaki T, Engelhardt M. Impact of recent research findings on eccentrically braced frame (EBF) design. *Proceedings of the 73rd Annual Convention*, *SEAOC*, Sacramento, CA, pp. 197–209, 2004.
4. Richards P, Uang C-M. Evaluation of rotation capacity and overstrength of links in eccentrically braced frames. *Report No. SSRP-2002/18*, Department of Structural Engineering, University of California, San Diego, La Jolla, CA, 2002.
5. Hibbitt, Karlsson and Sorensen. *ABAQUS User's Manual Version 6.2*. Hibbitt, Karlsson and Sorensen, Inc., Pawtucket, RI, 2001.
6. McDaniel CC, Uang CM, Seible F. Cyclic testing of built-up steel shear links for the New Bay Bridge. *Journal of Structural Engineering* (ASCE) 2003; **129**:801–809.
7. Dusicka P, Itani A, Buckle IG. Cyclic behavior of shear links and tower shaft assembly of San Francisco–Oakland Bay Bridge Tower. *Report No. CCEER 02-6*, Civil Engineering Department, University of Nevada, Reno, 2002.
8. Chou CC, Uang CM, Seible F. Compression testing of orthotropic steel deck for the new San Francisco–Oakland Bay self-anchored suspension bridge. *Report No. SSRP-2002/12*, Department of Structural Engineering, University of California, San Diego, La Jolla, CA, 2003.

